

Contribution to the Proceedings of the Charles U./JINR and International U. (Dubna)
CERN COMPASS Summer School,
Charles University, Prague, Czech Republic, August 1997,
Eds. M. Chavleishvili and M. Finger
Tel Aviv U. Preprint TAUP-2473-98
HEP-EX Archive <http://xxx.lanl.gov>, hep-ex/9801011

Primakoff Physics for CERN COMPASS Hadron Beam: Hadron Polarizabilities, Hybrid Mesons, Chiral Anomaly, Meson Radiative Transitions

Murray A. Moinester, Victor Steiner,
School of Physics and Astronomy,
R. and B. Sackler Faculty of Exact Sciences,
Tel Aviv University, 69978 Ramat Aviv, Israel
e-mail: murraym@silly.tau.ac.il, steiner@gluon.tau.ac.il

Abstract

We describe a hadron physics program attainable with a partially instrumented CERN COMPASS spectrometer, involving tracking detectors and moderate-size ECAL2/HCAL2 calorimeters. COMPASS can realize a state-of-the-art hadron beam physics program based on hadron polarizability, hybrid mesons, chiral anomaly, and meson radiative transition studies. We review here the physics motivation for this hadron beam program. We describe the beam, detector, trigger requirements, and hardware/software requirements for this program. The triggers for all this physics can be implemented for simultaneous data taking. The program is based on using a hadron beam (positive/negative pion, kaon, proton) in COMPASS.

1 Physics Review

The approved COMPASS physics program [1] includes studies of γ -hadron Primakoff interactions using 50-280 GeV/c negative beams (pions, kaons) and positive beams (pions, kaons, protons) together with a virtual photon target in dedicated data runs. Pion and kaon and proton polarizabilities, hybrid mesons, the chiral anomaly, and radiative transitions can be studied in this way, and can provide significant tests of QCD and chiral perturbation theory (χ PT) predictions. All of these subjects may be studied at the same time. Some COMPASS studies given in this report also appear in Refs. [2, 3].

1.1 Hadron Polarizabilities

For the γ - π interaction at low energy, chiral perturbation theory (χ PT) provides a rigorous way to make predictions; because it stems directly from QCD and relies only on the solid assumptions of spontaneously broken $SU(3)_L \times SU(3)_R$ chiral symmetry, Lorentz invariance and low momentum transfer. Unitarity is achieved by adding pion loop corrections to lowest order, and the resulting infinite divergences are absorbed into physical (renormalized) coupling constants L_i^r (tree-level coefficients in $L^{(4)}$, see Refs. [4, 5]). With a perturbative expansion of the effective Lagrangian limited to terms quartic in the momenta and quark masses ($O(p^4)$), the method establishes relationships between different processes in terms of the L_i^r . For example, the radiative pion beta decay and electric pion polarizability are expressed as [4]:

$$h_A/h_V = 32\pi^2(L_9^r + L_{10}^r); \bar{\alpha}_\pi = \frac{4\alpha_f}{m_\pi F_\pi^2}(L_9^r + L_{10}^r); \quad (1)$$

where $F_\pi = 93.1$ MeV [6] is the pion decay constant, h_A and h_V are the axial vector and vector coupling constants in the decay, and α_f is the fine structure constant. The experimental ratio [6] $h_A/h_V = 0.45 \pm 0.06$, leads to $\bar{\alpha}_\pi = -\bar{\beta}_\pi = 2.7 \pm 0.4$, where the error shown is due to the uncertainty in the h_A/h_V measurement [7]. **All polarizabilities in this paper are expressed in Gaussian units of 10^{-43} cm³.**

Holstein [8] showed that meson exchange via a pole diagram involving the $a_1(1260)$ resonance provides the main contribution ($\bar{\alpha}_\pi = 2.6$) to the polarizability. COMPASS can obtain new high statistics data for radiative transitions leading from the pion to the $a_1(1260)$, and to other meson resonances.

In fact, the $a_1(1260)$ width and the pion polarizability are related to an interesting question, which is whether or not one can expect gamma ray rates from the quark gluon plasma to be higher than from the hot hadronic gas phase in relativistic heavy ion collisions. Xiong, Shuryak, Brown (XSB) calculate photon production from a hot hadronic gas via the reaction $\pi^- + \rho^0 \rightarrow \pi^- + \gamma$. They assume that this reaction proceeds through the $a_1(1260)$. For $a_1(1260) \rightarrow \pi\gamma$, the experimental width [9] is $\Gamma = 0.64 \pm 0.25$ MeV. Xiong, Shuryak, and Brown (XSB) [10] estimate this radiative width to be $\Gamma = 1.4$ MeV, more than two times higher than the experimental value [9]. With this estimated width, they calculate the pion polarizability to be $\bar{\alpha}_\pi = 1.8$. COMPASS can experimentally check the a_1 dominance assumption of XSB, and the consistency of the expected relationship of this radiative width and the pion polarizability [11].

For the kaon, χ PT predicts [2, 8, 12, 13, 14] $\bar{\alpha}_{K^-} = 0.5$. The kaon polarizability measurements at COMPASS should complement those for pion polarizabilities for chiral symmetry tests away from the chiral limit. A more extensive study of kaon polarizabilities

was given recently by Ebert and Volkov [15]. Until now, only an upper limit [16] at 90% confidence was measured (via energy shifts in heavy Z kaonic atoms) for the K^- , with $\bar{\alpha}_K \leq 200$.

The polarizabilities can be obtained from precise measurements of the γ -hadron Compton scattering differential cross sections. Antipov et al. [17] measured the $\gamma\pi$ scattering with 40 GeV pions via radiative pion scattering (Bremsstrahlung) in the nuclear Coulomb field

$$\pi^- + Z \rightarrow \pi^{-'} + Z' + \gamma \quad (2)$$

where Z is the nuclear charge. Fig. 1 defines the kinematic variables for such an experiment. The four-momentum of each particle in Eq. 2 is p_1 , p_2 , p_1' , p_2' , k' , respectively. In the one-photon exchange domain, this reaction is equivalent to $\gamma + \pi \rightarrow \gamma' + \pi'$, and the four-momentum of the incident virtual photon is $k = p_2 - p_2'$. We have therefore $t = k^2$ with t the square of the four-momentum transfer to the nucleus, $F(t)$ the nuclear form factor (essentially unity at small t , \sqrt{s} the mass of the $\gamma\pi$ final state. The t is larger than t_0 , the minimum value of t to produce a mass \sqrt{s} , see Section 2.2 for details. The momentum modulus $|\vec{k}|$ (essentially equal to p_T) of the virtual photon is in the transverse direction, and is equal and opposite to the momentum p_T transferred to the target nucleus. The final state γ and pion were detected in coincidence. The data selection criteria required one photon and one charged particle in the final state, their total four momenta consistent with that of the beam, small four momentum transfer t to the target nucleus, software cuts on the invariant energy of the final state $\pi\gamma$ system that are equivalent to choosing effective γ energies of 100–600 MeV in the pion rest frame (designated hereafter as anti-lab frame or "alab"), and other position, angle, and energy/momentum conditions.

The virtual photon with four-momentum $k = \{\omega, \vec{k}\}$ has virtual mass $M^2 = k^2 = t = \omega^2 - |\vec{k}|^2$. Since $t = 2M_Z[M_Z - E(Z', \text{lab})] < 0$, the virtual photon mass is imaginary. To approximate real pion Compton scattering, the virtual photon may be taken to be almost real. The COMPASS trigger and projected statistics will provide data over effective γ energies of 100–2000 MeV in the alab frame. Such an energy range compared to Antipov et al. allows significantly increased sensitivity to the polarizabilities. Good resolution in t is important, since the characteristic signature for Primakoff scattering is low- t , while the scattering through other processes such as meson and Pomeron exchange have larger t . Antipov et al. [17] measured the pion electric polarizability $\bar{\alpha}_\pi$ with low statistics (~ 7000 events) and found $\bar{\alpha}_\pi = 6.8 \pm 1.4(\text{stat}) \pm 1.2(\text{syst})$ [17]. This result included the assumption that $\bar{\alpha}_\pi + \bar{\beta}_\pi \approx 0.4$, based on dispersion sum rules [18]. The value 6.8 reported is far from the χ PT prediction. More precise measurements of experimental polarizabilities are needed in order to subject the chiral perturbation techniques of QCD to new and serious tests.

1.2 Hybrid Mesons

The hybrid ($q\bar{q}g$) mesons, along with glueballs (gg) are one of the most amazing consequences of the non-abelian nature of QCD. Detection of these exotic states is a long-standing experimental puzzle. The most popular approach for the hybrids search is to look for the "oddballs" - mesons with the quantum numbers not allowed for the $q\bar{q}$ states, for example $J^{PC} = 1^{-+}$, decaying to $\eta\pi$, $\eta'\pi$, $f_1(1285)\pi$, $b_1(1235)\pi$, etc.

From more than a decade of experimental efforts at IHEP [21, 22, 23], CERN [25], KEK [24] and BNL [20], several hybrid candidates have been identified. The most recent information came from BNL E852 experiment [20] which studied π^-p interaction at 18 GeV/c. They reported $J^{PC} = 1^{-+}$ resonant signals in $\eta\pi^-$ and $\eta\pi^0$ systems as well as

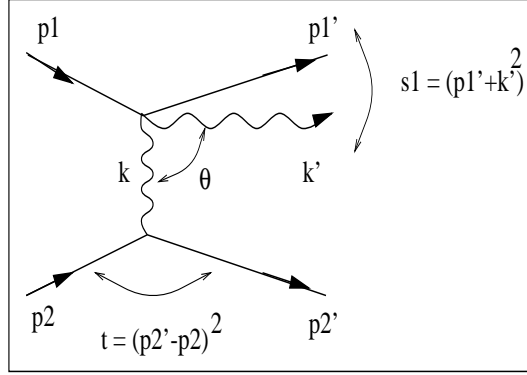


Figure 1: The Primakoff γ -hadron Compton process and kinematic variables (4-momenta): $p_1, p_1' =$ for initial/final hadron, $p_2, p_2' =$ for initial/final target, $k, k' =$ for initial/final gamma, and θ the scattering angle of the γ in the lab frame.

in $\pi^+\pi^-\pi^-$, $\pi^-\pi^0\pi^0$, $\eta'\pi^-$ and $f_1(1285)\pi^-$. At the same time, a VES group [23] has published analysis of $\eta\pi^-$, $\eta'\pi^-$, $f_1(1285)\pi^-$, $b_1(1235)\pi^-$ and $\rho\pi^-$ systems production in π^-Be interaction at 37 GeV/c. Although the $J^{PC} = 1^{-+}$ wave is clearly seen by VES in all channels, there is no indication for the presence of narrow ($\Gamma \sim 0.2$ GeV) resonance in any of them. But an observed abnormally high ratio of $\eta'\pi$ to $\eta\pi$ P-wave is considered as an evidence on hybrid nature of this exotic wave.

It should be mentioned that the partial wave analysis (PWA) of systems such as $\eta\pi$ or $\eta'\pi$ in the mass region below 2 GeV is particularly difficult. This is so because (1) this region is dominated by the strong 2^+ "background" (a_1 resonance), and (2) that the PWA may give ambiguous results [22] for the weaker 1^{-+} wave. The problem is that the PWA of the $\eta\pi$ system must take into account S, P and D waves, and the number of observables is not sufficient to solve unambiguously all equations. Looking at the partial wave solutions as a function of mass, each partial wave can have as many as eight different curves to describe its strength and phase, as discussed in ref. [22]. It is therefore extremely important to have extra information from different hybrid production mechanisms where the physics is different and such ambiguities may look different. Only by comparing results of different experiments in this way, can we establish unambiguously the existence or non-existence of hybrid (or exotic) meson states.

COMPASS can contribute significantly to the further investigation of hybrids by studying Primakoff production of $J^{PC} = 1^{-+}$ $\tilde{\rho}$ hybrids. The possibilities for Primakoff production of the $\tilde{\rho}$ with energetic pion beams, and detection via different decay channels has been discussed by Zielinski et al. [19], and Monte Carlo simulations for this physics were carried out for the 600 GeV FNAL SELEX run [19]. Considering vector dominance models, if the $\tilde{\rho}$ has a 1-10 MeV branching width into the $\pi\rho$ channel, a branching width of $\tilde{\rho}$ into the $\pi\gamma$ channel should be 3-30 keV [19]. A hybrid state with such a large radiative width would be produced at detectable levels through the Primakoff mechanism in COMPASS. A $\gamma - \pi$ COMPASS trigger should allow observation of the $\tilde{\rho}$ via the $\eta\pi^-$ decay mode. With a relative P wave ($L=1$), the $\eta\pi^-$ system has $J^{PC} = 1^{-+}$. The other decay channels of $\tilde{\rho}$ may be studied simultaneously in COMPASS by a relatively simple particle multiplicity trigger (say, three charged particles in final state).

The evidence presented for the hybrid (pionic) meson offers COMPASS an exceptional opportunity to take the next steps in this exciting field. COMPASS can study hybrid meson

candidates near 1.4 GeV produced by the Primakoff process. COMPASS should also be sensitive to pionic hybrids at higher excitation, and also to kaonic hybrids, which have not yet been reported. We may obtain superior statistics for a hybrid state if it exists, and via a different production mechanism without possible complication by hadronic final state interactions. We may also get important data on the different decay modes for this state. The observation of this hybrid in different decay modes and in a different experiment would constitute the next important step following the evidence so far reported.

COMPASS can provide a unique opportunity to investigate QCD exotics, glueballs and hybrids, produced via different production mechanisms: central production for glueballs and Primakoff production for hybrids. Taking into account the very high beam intensity, fast data acquisition, high acceptance and good resolution of the COMPASS setup, one can expect from COMPASS the highest statistics and a "systematics-free" data sample that includes many tests to control possible systematic errors. The COMPASS effort should significantly improve our understanding of hybrid and glueball physics.

1.3 Chiral Axial Anomaly

The Chiral Axial Anomaly can also be studied with 50-280 GeV pion beams with the same $\pi\gamma$ trigger as used above. For the γ - π interaction, the $O(p^4)$ chiral lagrangian [4, 5] includes Wess-Zumino-Witten (WZW) terms [40, 41], which lead to a chiral anomaly term [28, 40, 41] in the divergence equations of the currents. This leads directly to interesting predictions [41] for the processes $\pi^0 \rightarrow 2\gamma$ and $\gamma \rightarrow 3\pi$; and other processes as well [41]. The two processes listed are described by the amplitudes F_π and $F_{3\pi}$, respectively.

The chiral anomaly term leads to a prediction for F_π and $F_{3\pi}$ in terms of N_c , the number of colors in QCD; and f , the charged pion decay constant. The $O(p^4)$ F_π prediction is in agreement with experiment [41]. The $F_{3\pi}$ prediction is [27, 26]:

$$F_{3\pi} = \frac{N_c(4\pi\alpha)^{\frac{1}{2}}}{12\pi^2 f^3} \sim 9.7 \pm 0.2 \text{ GeV}^{-3}, \quad O(p^4). \quad (3)$$

The experimental confirmation of this equation would demonstrate that the $O(p^4)$ terms are sufficient to describe $F_{3\pi}$.

The amplitude $F_{3\pi}$ was measured by Antipov et al. [28] at Serpukhov with 40 GeV pions. Their study involved pion production by a pion in the nuclear Coulomb field via the Primakoff reaction:

$$\pi^- + Z \rightarrow \pi^{-'} + \pi^0 + Z'. \quad (4)$$

In the one-photon exchange domain, Eq. 4 is equivalent to:

$$\pi^- + \gamma \rightarrow \pi^{-'} + \pi^0, \quad (5)$$

and the 4-momentum of the virtual photon is $k = p_Z - p_{Z'}$. The cross section formula for the Primakoff reaction depends on $F_{3\pi}^2$. The Antipov et al. data sample (roughly 200 events) covered the ranges $-t < 2. \times 10^{-3} \text{ (GeV/c)}^2$ and $s(\pi^- \pi^0) < 10. m_\pi^2$. The small t -range selects events predominantly associated with the exchange of a virtual photon, for which the target nucleus acts as a spectator. Diffractive production of the two-pion final state is blocked by G-parity conservation. The experiment [28] yielded $F_{3\pi} = 12.9 \pm 0.9 \text{ (stat)} \pm 0.5 \text{ (sys)} \text{ GeV}^{-3}$. This result differs from the $O(p^4)$ expectation by at least two standard

deviations; so that the chiral anomaly prediction at $O(p^4)$ is not confirmed by the available $\gamma \rightarrow 3\pi$ data.

Bijnens et al. [41] studied higher order χ PT corrections in the abnormal intrinsic parity (anomalous) sector. They included one-loop diagrams involving one vertex from the WZW term, and tree diagrams from the $O(p^6)$ lagrangian. They determine parameters of the lagrangian via vector meson dominance (VMD) calculations. The higher order corrections are small for F_π . For $F_{3\pi}$, they increase the lowest order value from 7% to 12%. The one-loop and $O(p^6)$ corrections to $F_{3\pi}$ are comparable in strength. The loop corrections to $F_{3\pi}$ are not constant over the whole phase space, due to dependences on the momenta of the 3 pions. The average effect is roughly 10%, which then increases the theoretical prediction by 1 GeV^{-3} . The prediction is then $F_{3\pi} \sim 10.7$, closer to the data. The limited accuracy of the existing data, together with the new calculations of Bijnens et al., motivate an improved and more precise experiment.

1.4 Meson Radiative Transitions

With the same trigger as needed for the above studies, we can also obtain new high statistics data for the radiative transitions of incident mesons to higher excited states; such as from the pion to the ρ^- and from the K^- to the K^{*-} . These radiative transition widths are predicted by vector dominance and quark models. For $\rho \rightarrow \pi\gamma$, the widths obtained previously [30, 31, 32] range from 60 keV to 81 keV. For $K^* \rightarrow K\gamma$, the widths obtained previously are $48 \pm 11 \text{ keV}$ [33] and $51 \pm 5 \text{ keV}$ [34]. Independent data for these and higher resonances would be valuable to get higher precision measurements to allow a more meaningful comparison with theoretical predictions.

With a particle multiplicity trigger, we will also obtain new high statistics data for radiative transitions leading from the pion to the $a_1(1260)$, and to the $a_2(1320)$, and to other resonances or exotics. These radiative transition widths were studied in the past by different groups by vector dominance and quark models, but independent data would still be of value. For $a_1(1260) \rightarrow \pi\gamma$, the width given [9] is $\Gamma = 0.64 \pm 0.25 \text{ MeV}$, and for $a_2(1320) \rightarrow \pi\gamma$, the width given [35] is $\Gamma = 0.30 \pm 0.06 \text{ MeV}$.

2 Experimental Requirements

We consider the beam, detector, trigger and financial requirements for polarizability, hybrid, and anomaly studies, beginning for illustration with pion polarizability measurements with a 300 GeV pion beam. Although our illustrative simulations are given at 300 GeV, the data run will actually be at the maximum convenient energy for the COMPASS beam line, closer to 280 GeV. The beam energy is chosen to be maximal, since that pushes the energy spectrum of final state γ 's, π^0 's, and η 's to be highest, and thereby the detection acceptance for η 's for a given size ECAL2 electromagnetic calorimeter will be maximal.

The reaction $\pi^- + Z \rightarrow \pi^- + \gamma + Z'$ is considered for illustration. Simulations of the other reactions in the COMPASS apparatus are in progress. The experimental setup is shown schematically in Fig. 2. In Fig. 5, we show the kinematics from our Monte Carlo [36] study of the measurement accuracy. Fig. 7 shows the acceptance for angular distribution measurements, due to various trigger conditions. In Fig. 6 we show various correlations between the π and γ kinematic variables in the lab frame. In Fig. 10 we show the important correlation between the scattering angle of the γ in lab frame (used to extract the polarizability) and the π and γ kinematic variables in the lab frame.

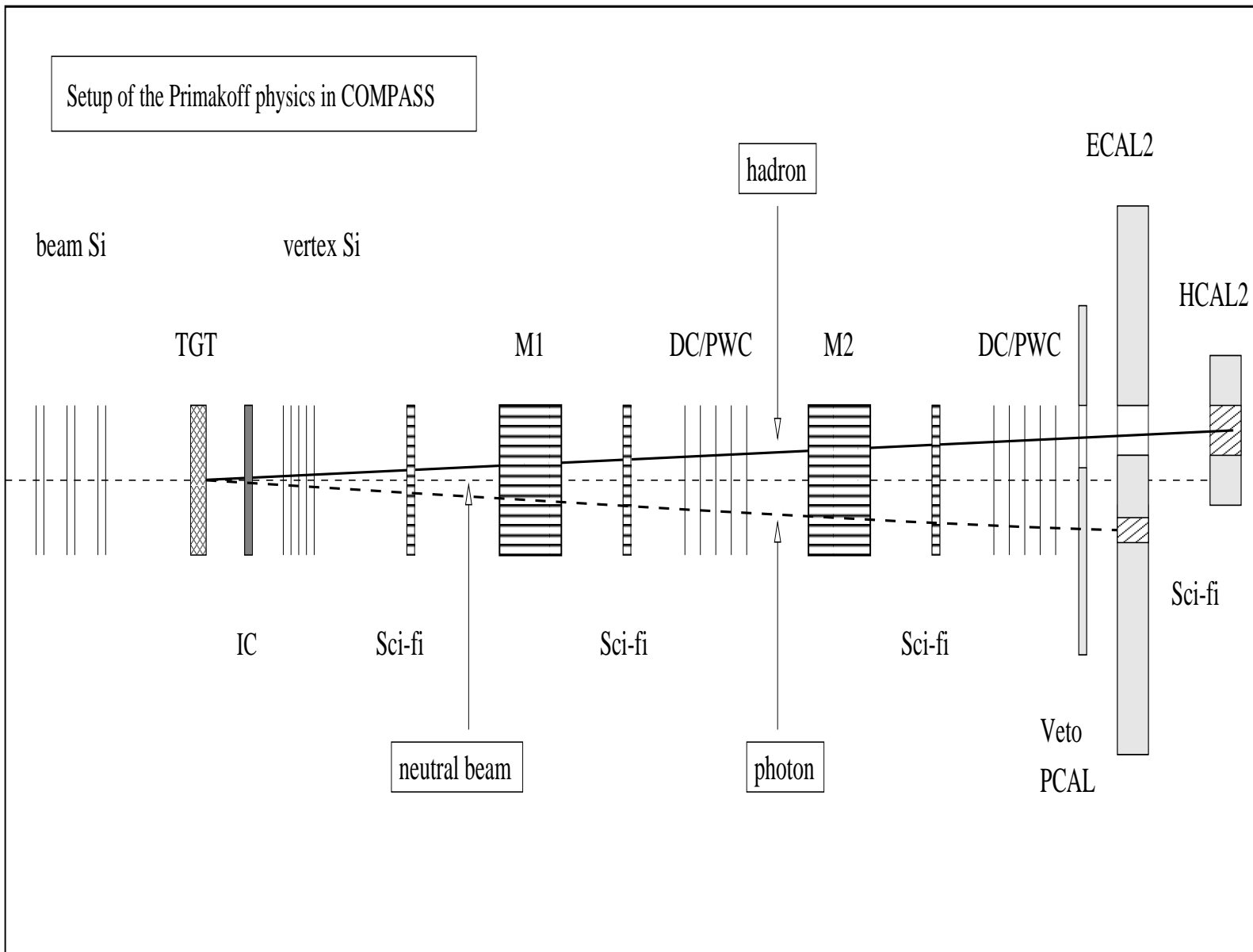


Figure 2: COMPASS setup for polarizability physics.

File	Function
polaris.f	source code
pol_pi_pb.inp	input data
polaris.dat	output event file in Geant-like format
events.dat	output binary event file for fast reruning
polaris.hbk	output histogram file
mkipol	to make the executable code
gopol	to run the code

Table 1: Description of input/output files for the Monte Carlo event generator POLARIS.

2.1 Monte Carlo Simulations

We have carried out Monte Carlo simulations with two codes, POLARIS, an event generator for polarizability studies and ANOMALY, developed for chiral anomaly studies[36]. In this report, we show only the POLARIS results. For hybrid mesons, simulations [19] were carried out for the SELEX apparatus, and need to be done now for COMPASS.

POLARIS produces events of type:

$$h + Z \rightarrow h' + \gamma + Z' \quad (6)$$

where h is a pion or kaon, based on the theoretical Primakoff γ -meson Compton scattering cross section. The meson and γ laboratory variables may be given gaussian spreads to simulate instrumental errors and acceptance cuts may be used (optional). Finally, the event is reconstructed from these "measured" values. The meson polarizability is extracted via a fit of the theoretical cross section to the scattered photon angular distribution in the projectile (alab) frame. The total cross section is computed by integrating numerically the differential cross section $\sigma(s,t,\theta)$ of the Compton process (see Fig. 1). The various techniques used are commented in the code. The relevant files are described in Table 1.

The code ANOMALY produces events of type:

$$h + Z \rightarrow h' + \pi^0 + Z' \quad (7)$$

where π^0 decays to 2γ , using similar techniques as POLARIS.

2.2 Primakoff $\gamma - \pi$ Compton Event Generator

We give more details regarding the event generator for the radiative scattering of the pion (pion Bremsstrahlung) in the Coulomb field of a nucleus [2, 13]. In the pion alab frame, the nuclear Coulomb field effectively provides a virtual photon beam incident on a pion target at rest. At small invariant momentum transfer $t \leq 10^{-4} \text{ (GeV/c)}^2$, where t equals the photon mass square, the virtual photons are quasi-real. In addition, the electromagnetic contribution to the scattering amplitude is large compared to meson exchange contributions. This allows one to measure the pion polarizability (a hadronic quantity) via a well understood QED probe.

The Primakoff differential cross section of this process in the alab frame may be expressed as [37]:

$$\frac{d^3\sigma}{dt d\omega d \cos \theta} = \frac{\alpha_f Z^2}{\pi \omega} \cdot \frac{t - t_0}{t^2} \cdot \frac{d\sigma_{\gamma\pi}(\omega, \theta)}{d \cos \theta}, \quad (8)$$

with the following expression for the $\gamma\pi$ cross section in the pion alab frame:

$$\frac{d\sigma_{\gamma\pi}(\omega, \theta)}{d\cos\theta} = \frac{2\pi\alpha_f^2}{m_\pi^2} \cdot \left\{ F_{\gamma\pi}^{pt}(\theta) + \frac{m_\pi\omega^2}{\alpha_f} \cdot \frac{\bar{\alpha}_\pi(1 + \cos^2\theta) + 2\bar{\beta}_\pi\cos\theta}{\left(1 + \frac{\omega}{m_\pi}(1 - \cos\theta)\right)^3} \right\}. \quad (9)$$

Here, $t_0 = (m_\pi\omega/p_b)^2$, with p_b the incident pion beam momentum in the laboratory, θ is the scattering angle of the real photon relative to the incident virtual photon direction in the alab frame, ω is the energy of the virtual photon in the alab frame, Z is the nuclear charge, m_π is the pion mass, α_f is the fine structure constant and $\bar{\alpha}_\pi$, $\bar{\beta}_\pi$ are the pion polarizabilities. The energy of the incident virtual photon in the alab (pion rest) frame is:

$$\omega \sim (s - m_\pi^2)/2m_\pi; \quad (10)$$

so that the energy of the photon is determined by s , the squared mass of the $\gamma\pi$ final state. The function $F_{\gamma\pi}^{pt}(\theta)$ accounts for the angular dependence of the point Thomson cross section, for scattering in a pure Coulomb field. For pion scattering, it reads:

$$F_{\gamma\pi}^{pt}(\theta) = \frac{1}{2} \cdot \frac{1 + \cos^2\theta}{\left(1 + \frac{\omega}{m_\pi}(1 - \cos\theta)\right)^2}. \quad (11)$$

From Eq. 9, the cross section depends on $(\bar{\alpha}_\pi + \bar{\beta}_\pi)$ at small θ , and on $(\bar{\alpha}_\pi - \bar{\beta}_\pi)$ at large θ . A precise fit of the theoretical cross section (Eq. 8-11) to the measured angular distribution of scattered photons, allows one to extract the pion electric and magnetic polarizabilities. Fits will be done for different regions of ω for better understanding of the systematic uncertainties. We will carry out analyses with and without the dispersion sum rule constraint that $\bar{\alpha}_\pi + \bar{\beta}_\pi \approx 0.4$. We can achieve a significantly smaller uncertainty for the polarizability by including this constraint in the fits. For fits without this constraint, the statistics requirement is a factor of 10-100 higher. Such unconstrained fits will also be of even greater interest.

The event generator produces events in the alab frame, characterized by three kinematical variables, t , ω and $\cos(\theta)$, and distributed with a probability, given by the theoretical Compton-Primakoff cross section (Eq. 8-11). Then, the photon-pion scattering kinematics are calculated. The virtual photon, specified by its four-vector components $k = \{\omega, \vec{k}\}$ and squared mass $t=M^2 = \omega^2 - |\vec{k}|^2$, incident along the recoil direction $\vec{k}/|k|$, is scattered on the pion "target" and emerges as a real photon with energy ω' at an angle θ :

$$\omega' = \frac{\omega\left(1 + \frac{\omega^2 - |\vec{k}|^2}{2m_\pi\omega}\right)}{1 + \frac{\omega}{m_\pi}\left(1 - \frac{|\vec{k}|}{\omega} \cos\theta\right)} \quad (12)$$

The photon azimuthal angle around the recoil direction is randomly generated using a uniform distribution. Afterwards, all four-vector components of all reaction participants (pion, photon and recoil nucleus) are calculated in the alab frame. The azimuthal angle of the recoil nucleus is also randomly generated by a uniform distribution. Finally, the reaction kinematics are transformed to the CM and then to the lab frame by a Lorentz boost.

For the measurement of the pion electric ($\bar{\alpha}_\pi$) and magnetic ($\bar{\beta}_\pi$) polarizabilities, one must fit the theoretical cross section (Eq. 8-11) to measured distributions, after correcting for acceptance losses. The dependence of the theoretical angular distributions on polarizability

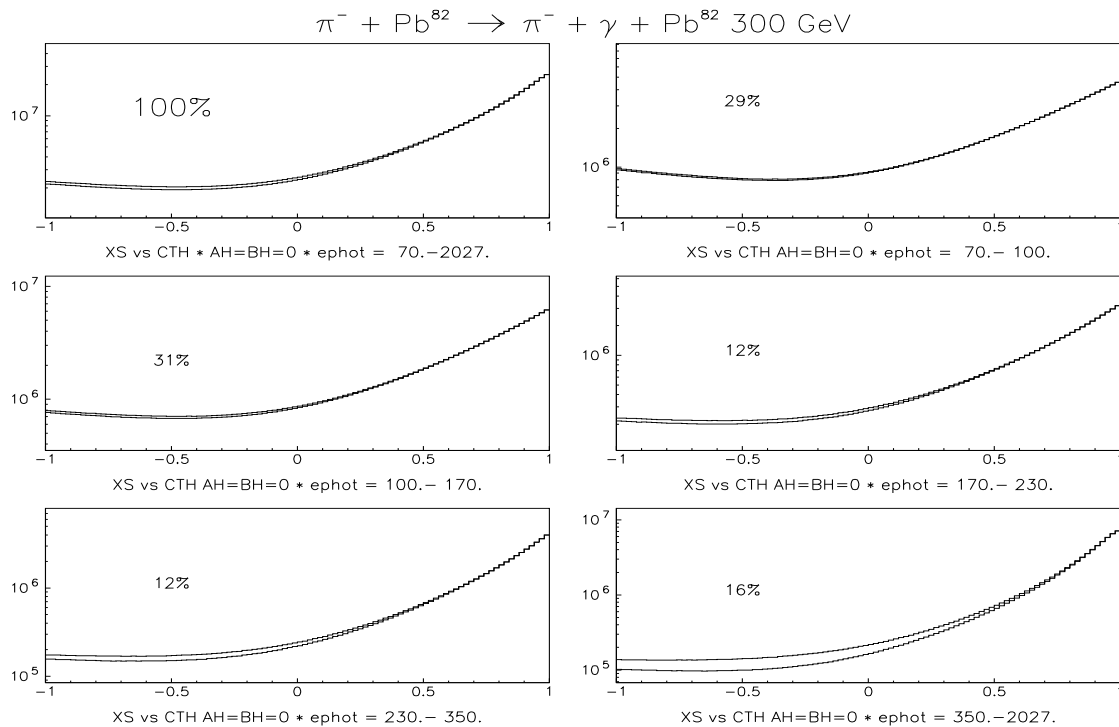


Figure 3: The dependence of the theoretical angular distributions on polarizability for different regions of γ energy ω (given in MeV), function of $\cos(\theta)$ in the alab frame. The lower curve corresponds to $\bar{\alpha}=7$, $\bar{\beta} = -6$; while the upper curve corresponds to zero polarizabilities. The percentage shows the statistics fraction in each ω region.

(for $\bar{\alpha} = 0, 6.8$) for different regions of γ energy ω in the alab frame is given in Fig. 3-4. The sensitivity to the polarizability increases with increasing ω energy and at back angles. We carried out several tests (a) by comparing the generated one-dimensional t , ω and $\cos(\theta)$ distributions (integrated over the other two variables) with the corresponding theoretical cross sections, (b) by comparing the Monte-Carlo computed total cross section with the theoretical value, given by numerical integration of Eq. 8-11, (c) by fitting the generated $\cos(\theta)$ event distribution with the theoretical cross section, and getting back the input values of $\bar{\alpha}_\pi$ and $\bar{\beta}_\pi$. A convenient method is to use the $\cos(\theta)$ distribution integrated over t and ω , which is most sensitive to the polarizability effect. We performed fits to this distribution in different ω regions, and for the entire ω domain. For the fit, we used a MINUIT routine, which minimizes the χ^2 statistic between the theoretical and measured points, with three free parameters: $\bar{\alpha}_\pi$, $\bar{\beta}_\pi$ and a normalization constant. The routine evaluates those parameters, as well as their statistical error. These tests ensured us that the simulated distributions are correct to a high degree of precision, as needed for the measurement of the polarizability with $\Delta\bar{\alpha}_\pi \approx 0.2$.

2.2.1 Design of the Primakoff Trigger

The small Primakoff cross section and the high statistics required for extracting the hadron polarizability requires a data run at high beam intensities with good acceptance. This sets the main requirements for the trigger system:

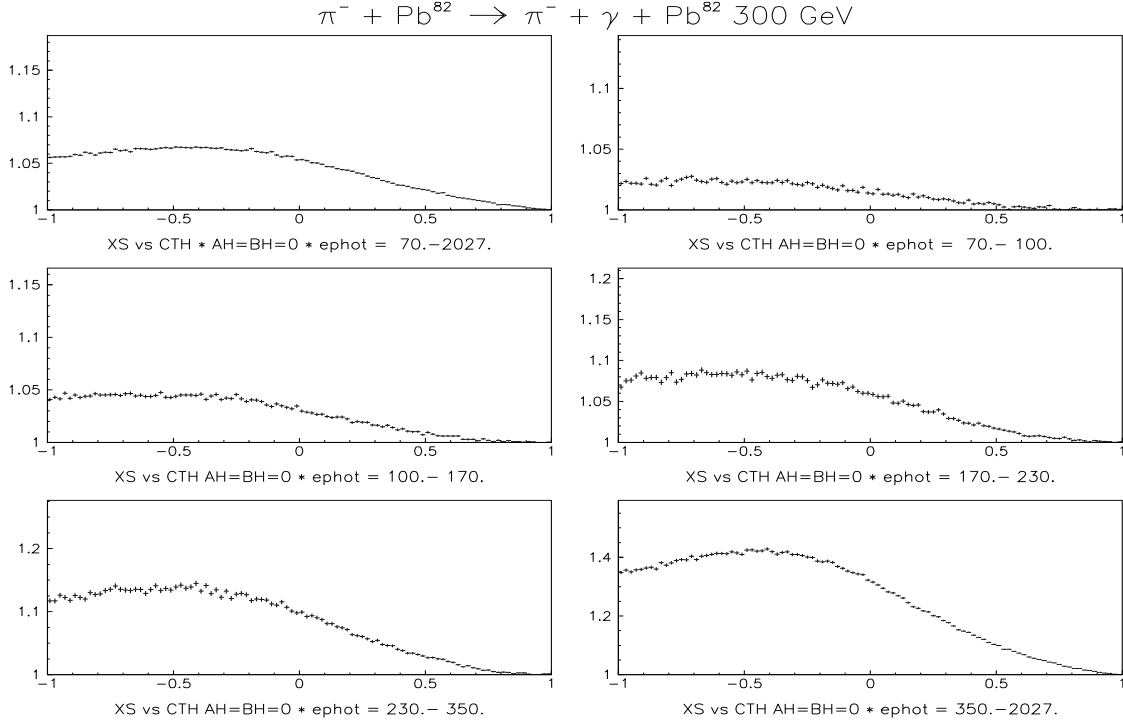


Figure 4: Ratio of the theoretical angular distributions for different regions of γ energy ω (given in MeV), as a function of $\cos(\theta)$ in the lab frame, for the case of zero polarizabilities (Thomson term only), relative to the case in which $\bar{\alpha} = 7$, $\bar{\beta} = -6$. The contribution of the polarizability to the cross section is larger at back lab angles, and increases with increasing ω .

- it has to act as a "beam killer" , to suppress the high rate background associated with non-interacting beam pions
- it has to avoid cutting the acceptance at the important photon back angles in the lab frame, where the hadron polarizability measurement is most sensitive.
- it has to cope with background from low energy γ 's or delta electrons caused by the beam passing through the apparatus.

We want to adapt a Primakoff trigger by a veto of the unscattered beam in a window on the hadron energy and a coincidence of the scattered pion with a γ measured in the calorimeter.

To study the feasibility of such a trigger scenario, simulations were carried out at 300 GeV, for illustrative purposes. The actual measurements will most likely be carried out at 280 GeV.

For the reaction given in Eq. 2 (at 300 GeV/c), the laboratory outgoing γ 's are emitted within an angular cone of up to 5 mrad, and the corresponding outgoing π 's are emitted up to 2 mrad. The γ energies range from 0 – 280 GeV, and the corresponding outgoing π energies range from 20 – 300 GeV. This is shown in the Figures 5, 7, 6 and 10. We consider the Compton scattering angular distribution in the lab frame. The recoil nucleus of mass M_T for a Primakoff reaction has negligible recoil energy ($T_r \approx t/2 M_T$), with

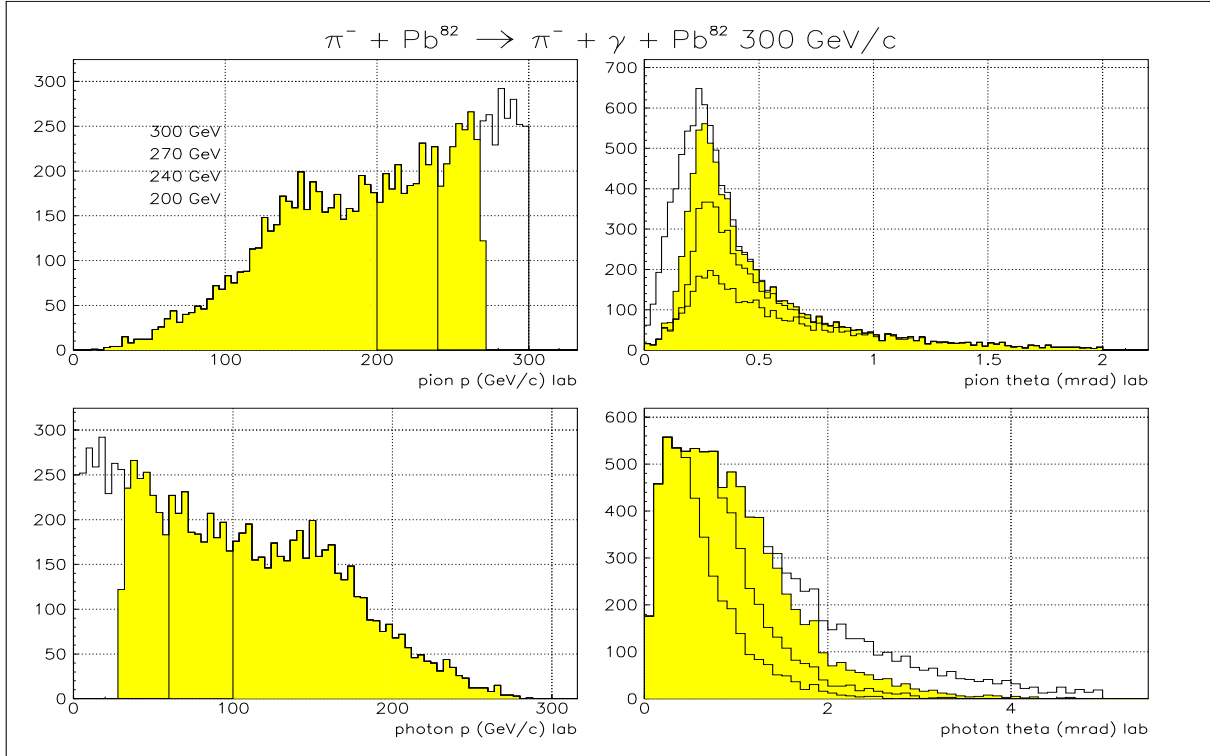


Figure 5: MC simulation showing the kinematics of the $\pi\gamma \rightarrow \pi\gamma$ reaction, in terms of the π and γ momenta and angles. The overlaid spectra correspond to different trigger cuts on the final state π momentum.

roughly 99% of the generated events having target recoil kinetic energies less than 30 keV. Therefore, the final state π and γ effectively carry all the four momentum of the beam pion, so that momentum and energy conservation may be used at the trigger level for background suppression.

For a 300 GeV pion beam, our Monte Carlo simulations (see Fig. 10) show that we lose very little polarizability information by applying an "energy cut" trigger condition that rejects events in which the final state charged pion has more than 240 GeV, and the final state γ has less than 60 GeV. The 240 GeV cut value was devised to act as a beam killer, as discussed in more detail below. The 60 GeV cut will also be very effective in reducing the γ detector (ECAL2) trigger rate, since a large part of the background γ rate for a 300 GeV beam energy is below 60 GeV.

The polarizability insensitivity to these cuts results from the fact that the most forward (in alab frame) Compton scattering angles have the lowest laboratory γ energies and largest laboratory angles. In addition, the cross section in this forward alab angle range is much less sensitive to the polarizabilities. This is seen from Eq. 11, since with $\bar{\alpha}_\pi + \bar{\beta}_\pi \approx 0$ from the dispersion sum rule, the polarizability component is small at forward compared with the back angles. The acceptance is reduced by the energy cut for the forward alab angles (shown in Fig. 7 for the alab frame), but is unaffected at the important alab back angles. In practice, the acceptance for alab $\cos(\theta) < -0.9$ will be reduced in off-line analysis, since this angular range corresponds to laboratory outgoing pion angles less than $100 \mu\text{rad}$. Such events will be rejected since their z position and momenta cannot be well determined in

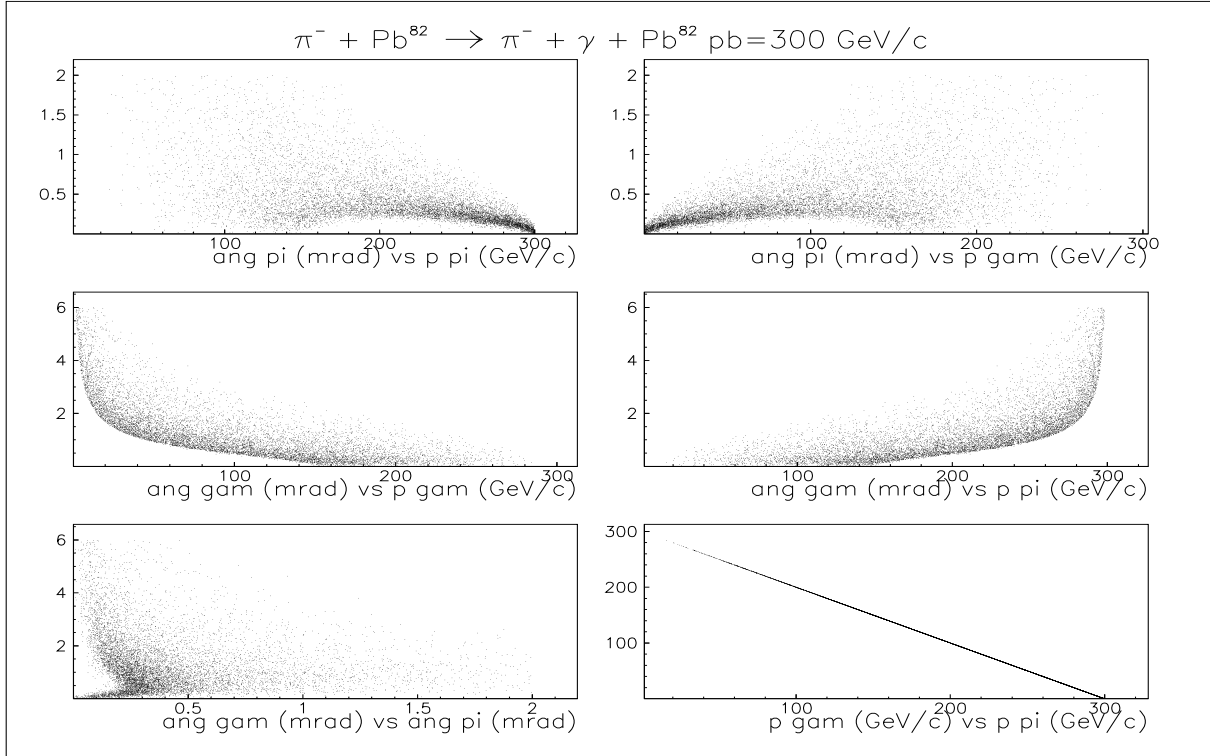


Figure 6: MC simulation showing the correlation between the π and γ kinematic variables in the lab frame.

part due to the $40 \mu\text{rad}$ angle measurement error from the Coulomb multiple scattering. However, the number of such events is limited, and their exclusion from the final fits should not significantly affect the polarizability determination. Summarizing, the purposes of the pion and γ energy constraints at the trigger level are fulfills the "beam killer" requirement and at the same time removes backgrounds associated with low energy γ 's or delta electrons or e^+e^- pairs incident on ECAL2,

Alternatively one might consider a trigger scenario based on a measurement of the track angles closed to the target. The SELEX/E781 [29] experiment at Fermilab used a mixed pion/hyperon beam at 600 GeV. The Primakoff physics in this experiment was attempted as a parasitic experiment, relative to the main charm topic. The charm trigger constraints did not allow implementing a $\gamma\pi$ coincidence condition for the first level trigger. SELEX therefore implemented a fast first level T1 "beam kill" Primakoff trigger, which did not include a signal from the gamma detector. Instead, the trigger worked by distinguishing pions with a small Primakoff scattering angle from non-interacting straight through beam pions. This trigger employed six (H,V) silicon planes grouped in 3 stations, two before and one after the target, with event-by-event readout. A processor provided a fast trigger for a scattering angle greater than $150 \mu\text{rad}$ at 250 nsec after beam crossing. In order to further reduce the DAQ rate, another trigger condition was required at the later T2 level. For this purpose, SELEX used a minimal energy deposit trigger of 100 GeV from the photon detector located 50 meters downstream. It was built by electronically summing up and then applying a discriminator to the signals of about 300 PbG blocks.

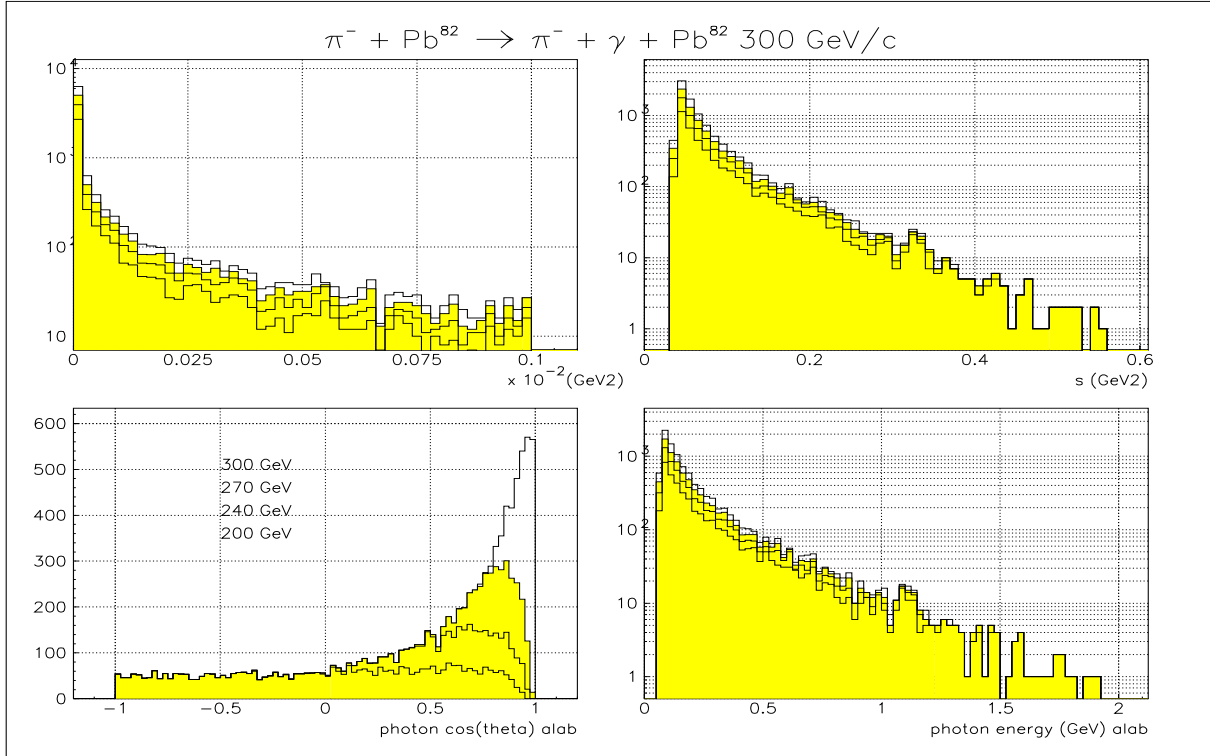


Figure 7: MC simulation showing the acceptance of the $\pi\gamma \rightarrow \pi\gamma$ reaction in terms of the invariant four momentum transfer t to the target, the squared invariant energy s of the final state $\pi\gamma$, the angular distribution versus $\cos(\theta)$ with θ the gamma scattering angle in the alab frame, and the virtual photon energy in the alab frame. The overlaid spectra correspond to different cuts on the final state π momentum.

As seen from the simulation in Fig. 8, the scatter angle trigger technique cuts the acceptance in the back angle range. Therefore, acceptance corrections and their uncertainties would be required for analysis of data taken with such a trigger. SELEX to this date was only able to have limited statistics dedicated data runs for the $\pi\gamma$, $\pi\pi^0$, $\pi\eta$ Primakoff final states.

We also considered a Primakoff trigger solution for COMPASS based on an position cut on the unscattered beam spot, at the maximal possible distance downstream, at the photon detector position. We carried out a Monte Carlo simulation in which we generated Primakoff events using the beam phase space from the Fermilab SELEX beam. The COMPASS beam properties given in Table 2 are somewhat better. The SELEX beam had a spot size on target of about 1 cm^2 and a divergence of about 1 mrad. The divergence is thereby larger than the average Primakoff angle, which literary places the Primakoff events "in the beam". We took into account the COMPASS magnetic deflection and considered a cut of about $8 \times 8 \text{ cm}^2$ over the beam spot at 40 meters downstream from target, where the COMPASS photon detector may be positioned. In the Fig. 9 upper plots, we compare the beam spot of the unscattered beam with the area covered by Primakoff events generated with the same beam phase space. We note the large overlay, which results in a considerable cut on Primakoff events. In the lower plots we show the photon alab $\cos(\theta)$ distribution before and after this cut. We note the important acceptance cut, due to alab back scattered photons hitting

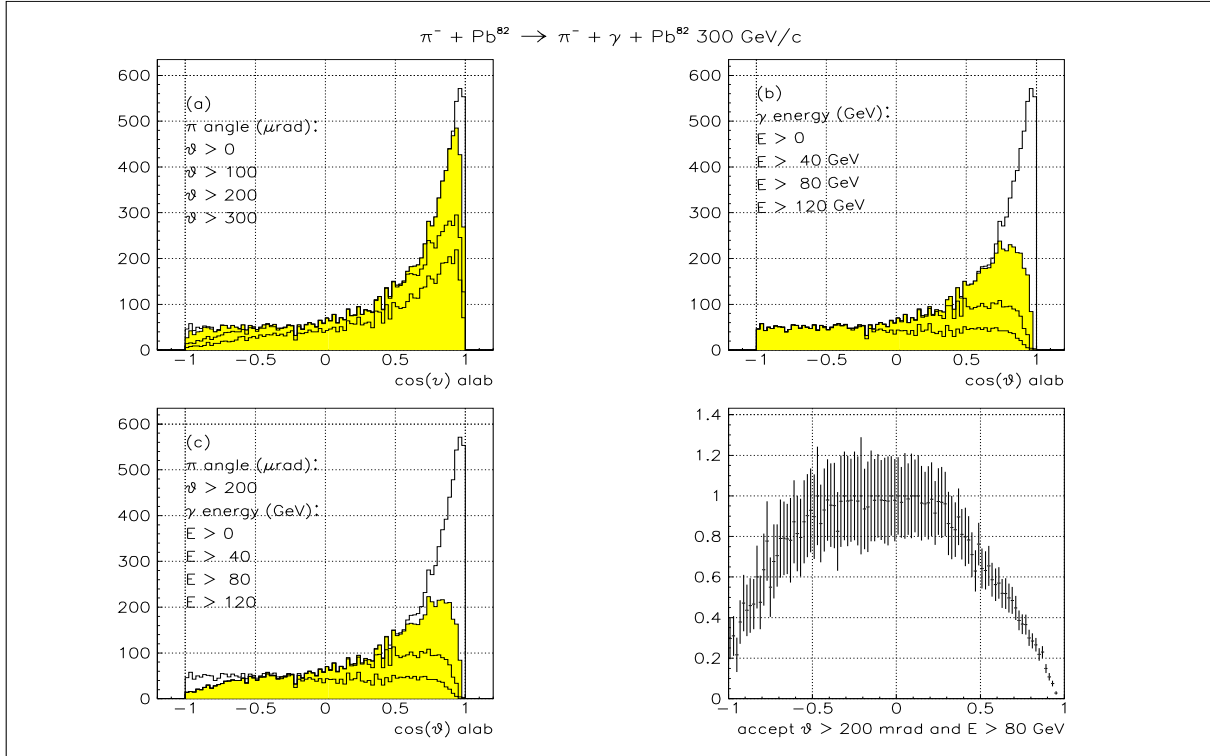


Figure 8: Monte Carlo simulation showing the acceptance in the photon scattering angle $\cos(\theta)$ in alab frame for: (a) cuts on the pion lab scattering angle, (b) cuts on the gamma lab energy, and (c) a combination of (a) and (b). The last plot shown the acceptance after these cuts. The $\cos(\theta)$ range in which the acceptance is essentially equal to 1 is very limited.

the beam veto area, which (as in the case above) would result in uncertain acceptance corrections.

2.3 Beam Requirements

The beam requirements for COMPASS Primakoff runs are given in Table 2. Two beam Cherenkov detectors (CEDARS) far upstream of the target provide $\pi/K/p$ PID. The incoming hadron momentum is measured in the beam spectrometer. Before and after the target, charged particles are tracked by high resolution silicon strip tracking detectors. The final state hadron and γ momenta are measured downstream in the magnet and in the photon calorimeter, respectively. This allows a precise determination of the small p_T kick to the target, the main signature of the Primakoff process, and the means to separate Primakoff from diffractive scattering.

The measurement of both initial and final state momenta provides constraints to identify the reaction. Since beam particles are identified in the CEDARS, and since we study simple exclusive reactions, there is no need for PID in the final state via a RICH. We can get quality statistics for the pion study with beam intensities of 5 MHz (1.25×10^7 particles in a 2.5 second spill) Some of the detectors (such as HCAL2 modules with a signal duration of about 50 nsec) needed for this study must accept the full beam intensity, and cannot tolerate beam intensities higher than 5 MHz. Beam rates lower than the final COMPASS rates are planned for this study, in which many of the COMPASS systems (DAQ, detectors, etc.) must be

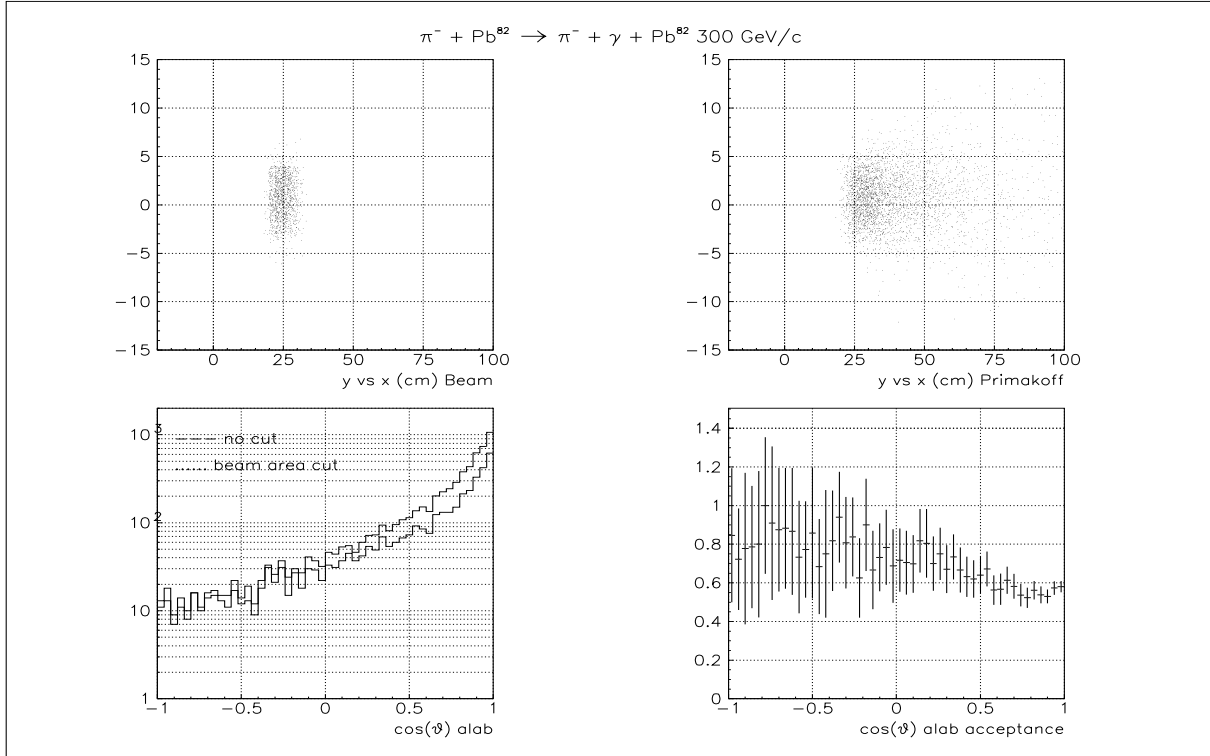


Figure 9: Monte Carlo simulation showing the acceptance in the photon scattering angle $\cos(\theta)$ in alab frame in the case of a cut on the beam (x,y) spot at the photon detector position. Upper left: pure beam spot with magnetic deflection (without target). Upper right: area covered by Primakoff events. Lower left: $\cos(\theta)$ distribution before and after a (x,y) cut on the beam spot. Lower right: $\cos(\theta)$ acceptance as ratio of the two spectra in the lower left plot. See the text for more details.

implemented. In this way, we proceed in a staged approach to study also the problems (dead time, pile up, radiation damage, etc.) associated with running with design beam intensities as high as 40 MHz. With the lower beam rates planned, we should also be able to achieve better beam quality. For example, we describe later that the electromagnetic calorimeter ECAL2 will have a hole in it (vertical size 7.6 cm, or 2 GAMS blocks) to allow all of the non-interacting beam and the main part of the Primakoff scattered pions (emitted at small laboratory angles) to pass through towards the hadron calorimeter HCAL2 located behind ECAL2. The beam should be tuned/collimated to be centered in this hole, with minimum halos. It is also important that data are taken with different beam energies and targets, as part of an effort to control systematic errors. Data should also be taken with both positive and negative beams (including proton beam).

2.4 Target and Target Detectors

The main Primakoff target will be Pb which has a 1.2 mb Compton scattering (polarizability) cross section and total inelastic cross section of 1.8 barn. We also need Primakoff scattering on nuclei with $Z < 82$ to see the Z^2 cross section dependence, and to make sure experimentally that there are no higher order corrections for atomic numbers as high as $Z=82$. We plan to arrange these targets along the beamline with a spacial distance large

Beam momentum (average)	300 GeV/c (or lower)
Momentum spread (rms)	13 GeV/c
Momentum resolution (rms)	2 GeV/c
Beam cycle	extraction 2.5 sec, total cycle 14.8 sec
Beam angular divergence (rms)	$\sigma_V = 0.5$ mrad, $\sigma_H = 0.5$ mrad
Beam particles	π^\pm , K, p
Beam particle ID	2 CEDARS (Cherenkov) in beam line
Beam intensity (part./spill)	$1.25 \cdot 10^7$

Table 2: Beam settings for Primakoff measurements.

enough, so that the target with the interaction can clearly be identified from the position of the kink in the pion trajectory (change in x,y slopes between beam and final state pion tracks)

With a 1% interaction length target, we expect roughly 80 $\pi\gamma$ events/spill for a beam of $2.5 \cdot 10^7$ pions/spill. Each Primakoff target is followed by two interaction counters (IC) with a triggering condition of 1 MIP each. We will check offline (not at the trigger level) that the detectors downstream of the targets (at different z-positions) have one charged particle. We need Si tracking detectors before and immediately after the targets. We veto target break-up events by selecting 1 MIP in the scintillation IC interaction counters after the targets, and by selecting low-t events in the off-line analysis. The target z-resolution (position) is less/more than ± 15 cm rms for events with outgoing pion scattering angles more/less than $100 \mu\text{rad}$.

2.5 The Magnetic Spectrometer and the t-Resolution.

We need good resolutions in momentum for the incident and final state pions and γ 's. Tracking before and after the magnet is required. In this way, the important four momentum resolution t (momentum transfer to the target nucleus) can be kept as good as possible. A final state π^- at 200 GeV/c can be momentum analyzed to 2 GeV/c resolution, with better resolution at lower momenta.

The angular resolution for the final state π should be good, which we may achieve by minimizing the multiple scattering in the targets and detectors. With a lead target of 1% interaction length = $2 \text{ g/cm}^2 = 0.30$ radiation length, the beam and outgoing pion multiple Coulomb scattering in the target gives an rms angular resolution of $40 \mu\text{rad}$. For this estimate, we assumed that a Primakoff 150 GeV pion is produced at the center of the target, and we added in quadrature the $18 \mu\text{rad}$ contribution of the incident 300 GeV pion and the $35 \mu\text{rad}$. contribution of the outgoing pion. We expect to have angular resolution not counting multiple scattering of about $6 \mu\text{rads}$ using for example $20 \mu\text{m}$ Si strips. This is based on an expected position resolution of $3 \mu\text{m}$ (using cluster centroid), and vertex planes 50 cm downstream from target. Thus, the vertex detector angular resolution is significantly better than the multiple scattering contribution to the angular resolution. We estimate the resolution of the transverse momentum p_T considering the p_T generated through MCS for a straight-through beam pion of 200 GeV. The p_T given to such a beam pion no Compton scattering) is then $p_T = p \times \Delta\theta = 200 \times 10^{-6} = 8 \text{ MeV}$, which corresponds $t = p_T^2 = 0.6 \times 10^{-4} \text{ GeV}^2$. Other contributions to the t-resolution are the

uncertainties in beam angle and momentum, detector material and air downstream of the target, and energy/position resolution in ECAL2. All together, we aim for a p_T resolution less than 15 MeV, corresponding to Δt better than $\approx 2.5 \times 10^{-4} \text{ GeV}^2$ over the energy range 40-240 GeV. These considerations fix the inherent Δt in determining $t = p_T^2$ for Primakoff Compton scattering.

Our resolution goal is based on the need for an effective t -cut to minimize contributions to the Coulomb data from diffractive production. We require a t -resolution that is about a factor of 10 smaller than the slope in t observed for diffractive data on a Pb target. The Pb diffractive data falls as $\exp(-t/0.0025)$ with t expressed in GeV^2 . This means that we need resolution $\Delta t=0.00025 \text{ GeV}^2$, or a resolution in transverse momentum less than 15 MeV. This conservative goal is based on the t distributions measured at a 200 GeV low statistics but high resolution experiment for $\pi^- \rightarrow \pi^- \pi^0$ [30] and $\pi^- \rightarrow \pi^- \gamma$ [38] Primakoff scattering at 200 GeV at FNAL. The t distribution of the $\pi^- \rightarrow \pi^- \gamma$ [38] data agrees well with the Primakoff formalism out to $t = 10^{-3} \text{ GeV}^2$, which indicates that the data is indeed dominated by Coulomb production.

In practice, we will study the t resolution and backgrounds in initial data runs. As part of our systematics studies, we plan to take some data with 0.5% rather than 1% interaction length Pb target. Minimum material (radiation and interaction lengths) in COMPASS will also give a higher acceptance, since that allows γ 's to arrive at ECAL2 with minimum interaction losses, while producing minimum e^+e^- backgrounds. That is, the fully instrumented COMPASS spectrometer is not needed. Only minimum equipment (the bare bones) should be used for this Primakoff physics, which also matches the constraints of a limited COMPASS budget.

2.6 The Photon Calorimeter ECAL2

The discussions for ECAL2 and HCAL2 follows our simulations, which were carried out at 300 GeV for illustrative purposes. The actual measurements will most likely be carried out at 280 GeV. In COMPASS, we can measure a final state 200 GeV γ to $\pm 2 \text{ GeV}$, with a position resolution of 1.5 mm, in the second photon calorimeter ECAL2. We plan to use an ECAL2 γ detector equipped with 3.8 by 3.8 cm^2 GAMS-4000 lead glass blocks to make a total circular active area of order 1.5 m diameter. The GAMS-4000 blocks are adequate. This is so, since radiation damage will be negligible for this run with beam intensity of at most 2.5×10^7 per spill. The hybrid meson study (η detection) sets the area of ECAL2.

The p_T kicks of the two COMPASS magnets are 0.45 GeV/c for SM1 (located 4 meters from target) and 1.2 GeV/c for SM2 (located 16 meters from target). We require the highest conveniently accessible effective p_T kick for this physics. The fields of both magnets must therefore be set *additive* for maximum deflection of the beam from the zero degree (neutral ray) line. We need to maximize the distance from the zero degree line to the beam hole in ECAL2 (located 40 meters or more from target), to attain at least 10 cm for the distance between the zero degree line and the hole edge. This is so since the Primakoff γ 's are concentrated around the zero degree line (see Fig. 10), and a good γ measurement requires clean signals from 9 blocks, centered on the hit block. The blocks near zero degrees should be selected to be the ones with the very best performance, and they should have accurate gain monitoring. ECAL2 should be at maximum distance from the target (we assume 40 meters) to also maximize the distance between the zero degree line and the deflected beam position at ECAL2. The hole size and position must be optimized to minimize the hadrons hitting ECAL2 blocks at the hole perimeter. We plan it to be big enough (2

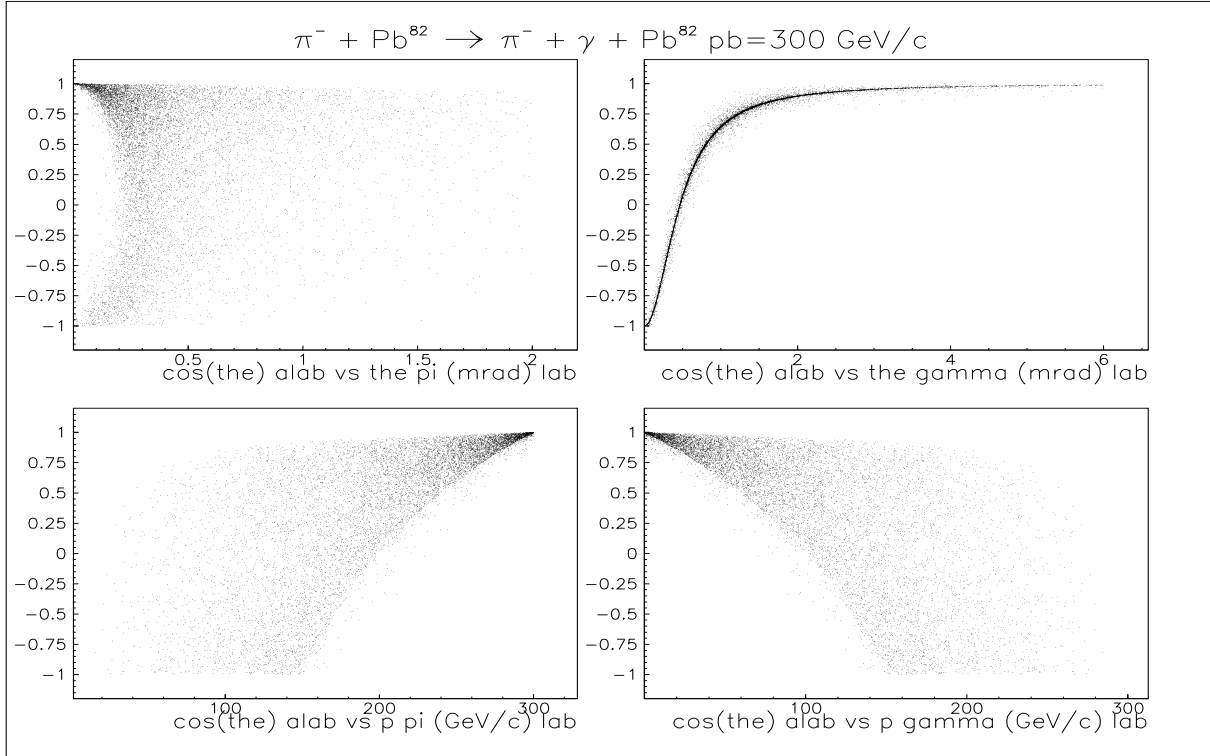


Figure 10: MC simulation showing the correlation between the $\cos(\theta)$ of the virtual photon in lab frame and the angles (upper plots) and momenta (lower plots) of the π and γ in the lab frame.

blocks $V \times 16$ blocks H) to pass completely the non-interacting beam, and to pass also the majority of Primakoff scattered pions. In that way, these particles are measured well in the HCAL2 hadron calorimeter behind ECAL2. We are then able to optimally fix the beam killer threshold cut. We may also better understand the detector behavior by comparing the energy determinations of tracking detectors and HCAL2, for those pions arriving at HCAL2 without traversing ECAL2.

Besides the polarizability $\pi\gamma$ detection, COMPASS should also detect $\pi\pi^0$ for the anomaly study and $\pi\eta$ for the hybrid study. The two γ 's from π^0 and η decay have opening angles $\theta_{\gamma\gamma}$ for the symmetric decays of $\theta_{\gamma\gamma} = m/4E_t$, where m is the mass (π^0 or η) and E_t is the lowest energy π^0 or η to be detected. And the opening angles are increased for the asymmetric decays. The π^0 's and η 's themselves are produced with an angular spread around the beam direction. The consequence is that to obtain good acceptance for all the Primakoff reactions discussed above, an ECAL2 with size of order 1.5 m diameter is required. This may be achieved with GAMS-4000 lead glass blocks, each of size 3.8×3.8 cm².

The 300 ± 13 GeV unscattered beam should be measured with HCAL2 to be between 240-360 GeV with 99% probability. From MC simulations, the number of Primakoff scattered pions below 40 GeV is less than 0.3%, so that 40 GeV pions are about the lowest energy of interest. In any case, too low energy pions may be blocked by the magnet yoke. We will effectively set a π^- acceptance energy window of 40 - 240 GeV, via a minimum threshold of 60 GeV for the γ energy deposited in ECAL2, and an HCAL2 veto for energies above 240

GeV. The size of the BP trigger scintillation detector (see section 2.8 below) must be of order $60 \times 15 \text{ cm}^2$ to accept unscattered beam and Primakoff scattered events. The vertical size of this BP detector is larger than the 10 cm needed for polarizability. It must match the anomaly and hybrid trigger, to catch also the scattered π^- 's associated with the $\pi^-\pi^0$ and $\pi^-\eta$ final states. Monte Carlo studies are in progress to optimize the vertical size of BP. The ECAL2 blocks will have their gains well matched, and their analog signals will be electronically summed and discriminated to provide a trigger signal on minimal energy deposit. In table 3 we show the ECAL2 contribution to the Primakoff trigger.

Primakoff physics requires a very good energy resolution of photon calorimeters. For the precise monitoring of the energy calibration of the photon calorimeters, COMPASS may use a dedicated laser system, which was built by the Tel-Aviv University group [39].

2.7 The Hadron Calorimeter HCAL2

We intend to use beam rates of order 5 MHz where the rate limit is the maximum allowed for good operation of the existing and tested $20 \times 20 \text{ cm}^2$ or $15 \times 15 \text{ cm}^2$ Dubna hadron calorimeter modules. For the beam killer trigger purposes, we require a mini-HCAL2 configured as an array of $15 \times 15 \text{ cm}^2$ blocks (2×2 or 3×3) to catch non-interacting beam pions. The energy sum for trigger purposes would be taken from this mini-HCAL2. However, we may use a larger HCAL2 array (matching the ECAL2 size) as an aid in PID and in fixing the HCAL2 threshold and as a check of the momentum determination by the tracking detectors. Such a large HCAL2 can give further understanding of events where a hadron hits ECAL2, and also for those that do not. The HCAL2 modules have energy resolution of $\pm 15 \text{ GeV}$ at 300 GeV. Together with the beam acceptance of $\pm 13 \text{ GeV}$, we can achieve a $1\text{-}\sigma$ identification of the beam via a detection window of $300 \pm 20 \text{ GeV}$. We can therefore set a $3\text{-}\sigma$ discriminator veto threshold at $300 - 3 \times 20 = 240 \text{ GeV}$, to veto 99% of the beam. We will reduce the beam acceptance to 13 GeV rms or lower, by collimation. With a lower threshold acceptance on HCAL2 (say 220 GeV), we may achieve a yet higher beam rejection. The final value of the energy cut will be set following in-beam tests. Here we just estimate that we will use HCAL2 to reject events with pion energies above 240 GeV for beam suppression. In table 3, we estimate the ECAL2/HCAL2 effect on the Primakoff trigger. The mini-HCAL2 modules will have their gains well matched, and their analog signals will be electronically summed and discriminated to provide a veto trigger signal for hadron energies above 240 GeV.

2.8 The Primakoff Trigger

We construct the Primakoff trigger using two to three trigger levels. The main setup elements involved in the trigger are shown in Fig. 11. For Primakoff physics, the trigger system electronics should ideally be localized in the region of the ECAL2 and HCAL2 calorimeters, so that the final trigger signals may be developed in the minimum time possible (to reduce dead time), and within the 300 – 1000 nsec allowed in the DAQ.

The T0 trigger is a fast logical signal defining the beam phase space, rate and purity at the target, and is generated near the target about 20 nsec after beam passage. It is produced via a logical relation between signals from an ensemble of beam transmission and beam halo veto (hole) scintillators located before the target. Cuts on the analog signals of the transmission scintillators should reject upstream interactions, beam spills with more than one particles, and thereby ensure a single incident hadron at the target per event. The

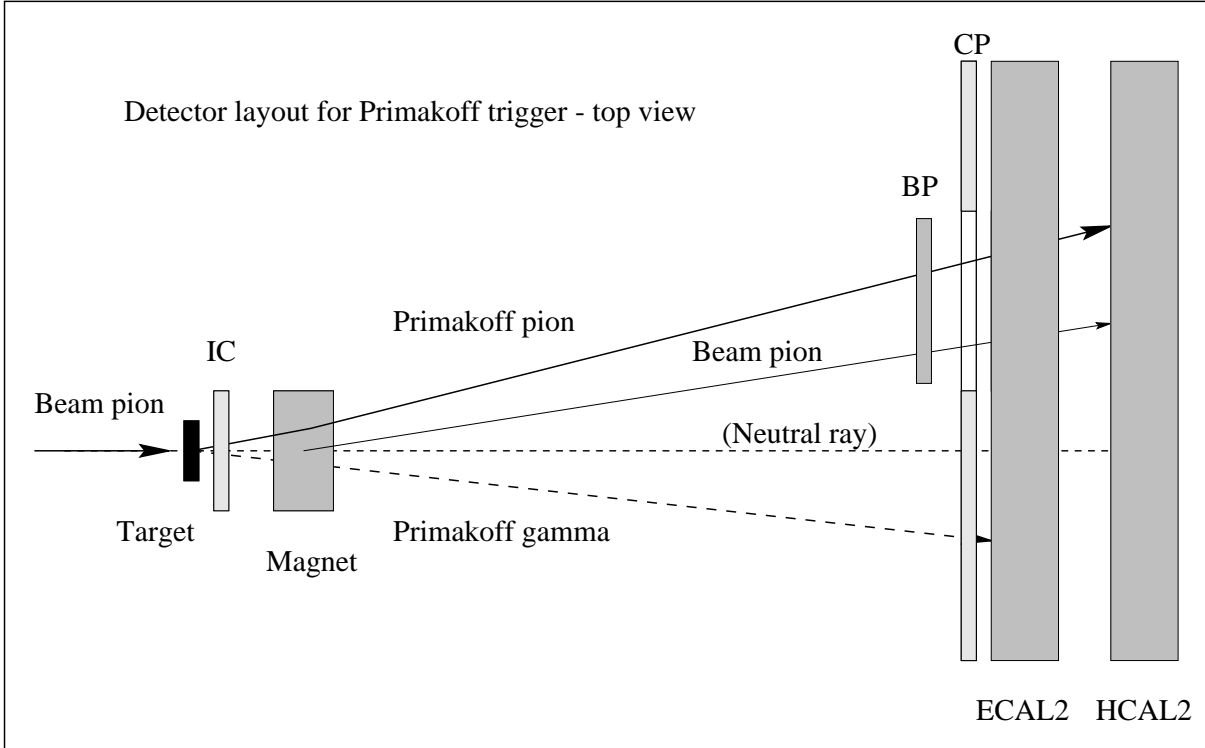


Figure 11: Detector layout for Primakoff trigger.

T0 trigger should ensure sufficient rate with a small beam size and with a beam divergence below 1 mrad rms. The size/divergence directly determines the performance of the T1 trigger downstream. For example, a beam divergence of 1 mrad rms at target projected 40 m downstream (without magnetic deflection) results in a beam spot size of 8 cm rms, and the stability of the spot size and position is also important.

The T1 trigger exploits the essential feature of a Primakoff polarizability (and also anomaly and hybrid) event: a coincidence between the γ and π detected in ECAL2 and a scintillator BP respectively. Fig. 11 shows the detectors participating in this trigger. Proceeding downstream, we consider the scintillation detectors IC (Interaction Counter), BP (Beam or Primakoff fiducial detector), CP (Charged Particle), and the photon/hadron calorimeters ECAL2/HCAL2. The phototube bases of all scintillators and IC counters should ensure gain stability at high counting rate.

The IC counter logical signal should correspond to an amplitude of 1 MIP. Using two successive IC counters allows an OR between their signals, which better accounts for the Landau distribution. In addition, with two IC counters, consistency and stability checks are possible.

BP is a scintillator fiducial paddle of dimensions 60 cm (in H) by 15 cm (in V), which is the size covered by the beam and the Primakoff scattering events (pions or kaons). BP is large enough in order to cover both the deflected beam and the scattered Primakoff particles. It includes the beam region, for the reasons discussed in section 2.2.1 above. BP helps form the pion detection trigger; it is set to fire on a 1 MIP window condition. To accommodate also the anomaly and hybrid triggers, the BP size was increased somewhat to account for the larger angular spread of the π^- 's from these channels. Simulations in

progress will help fix the definitive sizes of BP, CP, and the ECAL2 hole.

CP is a charged particle veto scintillator array positioned at the front face of ECAL2. It is designed with a hole slightly larger than the BP detector, in which the BP detector above is positioned. It covers the front face of ECAL2. CP protects ECAL2 from charged leptons or hadrons directed at them. Before we use CP, we will make measurements to assure that CP is unaffected by backscattered charged particles from ECAL2 and HCAL2. To reduce backscatter, one may possibly add some low Z material in front of ECAL2. We require an ECAL2 energy deposit above 60 GeV and an HCAL2 energy deposit below 240 GeV.

The first level trigger T1 is defined as:

$$T1 = IC(1 \text{ mip}) \cdot BP(1 \text{ mip}) \cdot \overline{CP} \cdot ECAL2(> 60 \text{ GeV}) \cdot \overline{HCAL2}(> 240 \text{ GeV}). \quad (13)$$

The trigger is designed to accept only events in which one Primakoff scattered pion hits and fires BP, the γ energy exceeds 60 GeV, and HCAL2 measures less than 240 GeV. All of the non-interacting pion beam and most of the Primakoff scattered pions pass through the ECAL2 hole (vertical size 7.6 cm, horizontal size 60 cm), and then no charged particle hits ECAL2 anywhere. These pions proceed to HCAL2, where their energy is measured well. Beam pions will then give HCAL2 signals greater than 240 GeV. Those Primakoff scattered pions that hit the blocks at the ECAL2 hole periphery (the wall of fire, or WOF) will lose some energy in ECAL2, and will not therefore have a good hadron energy measurement in HCAL2. We will reduce backgrounds associated with the tail of the beam hitting ECAL2 blocks on the WOF, by omitting these blocks from the ECAL2 sum signal. The ECAL2 low energy threshold is important to suppress low energy backgrounds and the electronic noise of the analog sum signals. In order to minimize electronic noise, both ECAL2 and HCAL2 summing circuits should use the techniques developed for this purpose of the GAMS experiment. This allows the noise level to be significantly lower than that given by the sum of all channels.

The task of the first level trigger T1 is to provide a fast gate signal to start digitization (for example in the ADC-system of the calorimeter) about ~ 300 ns after the beam traverses the target (see table 3). The rate of this signal ($2.5 \cdot 10^3$ per spill in table 3) will be significantly lower than the maximum of $1 \cdot 10^5$ per spill trigger rate accepted by the COMPASS data acquisition.

A second level trigger T2 can be constructed if a faster T1 or more rate reduction is needed. We will have a faster T1, if the IC counter 1 MIP trigger signal, which arrives the latest at ECAL2, will be transferred from T1 to T2. Further rate reduction may be gained using the additional trigger condition at T2 level. For example, a momentum determination from the pion direction near the target and behind SM2 can conceivably be integrated into the trigger scheme at a later stage, or at least be used as a cross check of the HCAL2 energy trigger. The T2 trigger should arrive no later than $\sim 1 \mu\text{sec}$ after the beam traverses the target.

Further data reduction may be done in the COMPASS filter farm, before writing to tape, using more detailed information from the tracking detectors and the ADCs.

2.9 Expected Trigger Rates

The ECAL2 γ signal above 60 GeV in coincidence with BP and with HCAL2 (40–240GeV) should reduce the trigger rate from the beam rate by a factor of 1000. The CP detector requirement should give at least another factor of 5 rate reduction. In this way, one may

Signature	Range	Timing (nsec)	Reduc. Fact.	Rate (events/spill)
Beam	–	0	–	$1.25 \cdot 10^7$
IC (interaction counter)	1 mip	1	–	$1.25 \cdot 10^7$
BP (beam or Primakoff)	1 mip	200	–	$1.25 \cdot 10^7$
CP (charged particles)	≥ 1 mip	200	5	$2.5 \cdot 10^6$
HCAL2 (π energy)	< 240 GeV	260	–	–
ECAL2 (γ energy)	> 60 GeV	260	1000	$2.5 \cdot 10^3$
			–	–

Table 3: The Primakoff trigger conditions and estimation of timing relative to the target crossing time, and trigger rate reduction. For HCAL2 and ECAL2 we consider coincidences and a common reduction factor.

expect to achieve a trigger rate lower than the beam rate by a factor of 5000. The resulting rate is 20 times lower than the maximum of 10^5 per spill DAQ limit in COMPASS.

We plan to study more precisely the background rates, and ways to reduce backgrounds. For this purpose, we will use an event generator for pion-nucleus interactions, embedded in the COMPASS apparatus. We will study what fraction of the events generated pass our trigger conditions. The factor 1000 reduction above is only a guess of what we expect from $\pi\gamma$ coincidence condition, with the energy ranges of table 3. The backgrounds will come from $\pi\gamma$ coincidences of non-Primakoff events, the rate of which depends on the ratio between the total inelastic and photon production cross sections in the target.

2.10 Measurement Significance

The Primakoff Compton cross section is 1.2 mbarn for Pb, while the the total inelastic cross section is 1.8 barn. For a COMPASS pion beam rate of 5 MHz (or $1.25 \cdot 10^7$ particles/spill see table 2), and a 1% interaction Pb target, we expect roughly 80 events/spill ($80 \approx 1.2/1.8 \times 10^{-3} \times 10^{-2} \times 1.25 \cdot 10^7$) from the pion Primakoff effect. This corresponds to 10^7 events per month at 100% efficiency. Assuming a trigger efficiency of 50% (due to the energy cuts), an accelerator operating efficiency of 50%, and a tracking efficiency of 80%, one may expect to observe $2 \cdot 10^6$ Primakoff Compton events per month. Statistics of this order will allow systematic studies, with fits carried out for different regions of t , s , photon energy ω , Z^2 , etc.; and polarizability determinations with statistical uncertainties of order 0.2 .

For the kaon polarizability, due to the lower intensity, the statistics will be roughly 50 times. A precision polarizability measurement requires more data taking time. Comparing chiral anomaly to polarizability data, we expect roughly 300 times statistics, due to the 140 times lower cross section and the lower π^0 efficiency ([27]). The detailed simulations and count rates expected for these channels will be presented in later reports.

3 Budget

We first consider the needs of the ECAL2 and HCAL2 calorimeters. To obtain good acceptance for all the Primakoff reactions discussed above, an ECAL2 with size of order 1.5 m diameter is required. The optimum size is under study. This may be achieved with GAMS-4000 lead glass blocks, each of size 3.8×3.8 cm². An HCAL2 calorimeter with 100

$20 \times 20 \text{ cm}^2$ Dubna cells can satisfy beam killer and PID functions. The ADC's for these blocks must be designed and built.

4 Conclusions

A hadron Primakoff physics program for COMPASS is proposed. The physics topics – measurement of the pion polarizability, search for hybrid meson(s), studies of the chiral anomaly and of radiative meson transitions – are discussed with emphasis on the pion polarizability, for which the simulations and detector studies are most advanced. The program can be achieved in a COMPASS run, using negative and positive hadron beams.

The proposed program can be run with a partially instrumented COMPASS spectrometer, consisting of the spectrometer magnets, the central tracking detectors, (parts of) the ECAL2/HCAL2 calorimeters and a relatively simple trigger. All physics topics proposed can be studied simultaneously.

5 Acknowledgments

This research was supported by the U.S.-Israel Binational Science Foundation research was supported by the U.S.-Israel Binational Science Foundation and the Israel Science Foundation founded by the Israel Academy Sciences and Humanities, Jerusalem, Israel. The authors thank M. Finger and M. Chavleishvili for the friendly atmosphere at the Charles U./JINR (Dubna)/International U. (Dubna) Prague COMPASS 1997 summer school. Thanks are due to M.P.I. Heidelberg SELEX/COMPASS group, U. Dersch, F. Dropmann, I. Eschrich, Kruger, J. Pochodzalla, B. Povh, J. Simon, and K. Vorwalter, for hospitality collaboration during the writing of this report. Thanks are due M. Buenerd, P. Cooper, D. Drechsel, T. Ferbel, L. Frankfurt, A. Ocheraschvili, S. Paul, J. Russ, I. Savin, H.W. Siebert, A. Singovsky, N. Terentyev, U. Wiedner, and T. Walcher for valuable discussions.

References

- [1] F. Bradamante, S. Paul et al., CERN Proposal COMPASS, <http://wwwcompass.cern.ch/>, CERN/SPSLC 96-14, SPSC/P 297.
- [2] M. A. Moinester, V. Steiner, Pion and Kaon Polarizabilities and Radiative Transitions, in Proceedings of the "Chiral Dynamics Workshop: Theory and Experiment", U. Mainz, Sept. 1997, Eds. A. Bernstein and T. Walcher, Springer-Verlag, 1998, hep-ex/9801008.
- [3] M. A. Moinester et al., COMPASS Draft Report, 1997, <http://vsnhd1.cern.ch/~murraym>.
- [4] J. F. Donoghue, B. R. Holstein, *Phys. Rev. D* **40**, 2378 (1989).
- [5] J. Gasser and H. Leutwyler, *Nucl. Phys. B* **250**, 465 (1985).
- [6] Particle Data Group, G. P. Yost et al., *Phys. Lett. B* **204**, 1 (1988); L. Montanet et al., *Phys. Rev. D* **50**, 1173 (1994).
- [7] D. Babusci, S. Bellucci, G. Giordano, G. Matone, A. M. Sandorfi, M. A. Moinester, *Phys. Lett. B* **277**, 158 (1992).
- [8] B. R. Holstein, *Comments Nucl. Part. Phys.* **19**, 239 (1990).
- [9] M. Zielinski et al., *Phys. Rev. Lett.* **52** (1984) 1195.
- [10] L. Xiong, E. Shuryak, G. Brown, *Phys. Rev. D* **46**, 3798 (1992).
- [11] M. A. Moinester, Pion Polarizability, Radiative Transitions, and Quark Gluon Plasma Signatures, Chiral Dynamics Workshop, M.I.T., July 1994, HEPPH-9410215.
- [12] M. A. Moinester, Proc., Conf. on the Intersections Between Particle and Nuclear Physics, Tucson, Arizona, AIP Conf. Proc. 243, P. 553, 1992, Ed. W. Van Oers.
- [13] M. A. Moinester, Pion and Sigma Polarizabilities and Radiative Transitions, in "Chiral Dynamics: Theory and Experiment", Eds. A. Bernstein and B. Holstein, Springer-Verlag, QC793.3.C54C48, 1995, HEPPH-9409463.
- [14] M. Buenerd, *Nucl. Instr. Meth.* **A136** (1995) 128.
- [15] D. Ebert, M. K. Volkov, *Phys. Atom. Nucl.* **60**, 796 (1997).
- [16] G. Backenstoss et al., *Phys. Lett. B* **43**, 431 (1973).
- [17] Y. M. Antipov et al: *Phys. Lett. B* **121** 445 (1983); Y. M. Antipov et al: *Z. Phys. C-Particles and Fields* **26** 495 (1985).
- [18] J. Portales, M. R. Pennington, Theoretical Prediction of pion polarizabilities, DAΦNE Physics Handbook, hep-ph/9407295.
- [19] M. Zielinski et al., *Zeit. Phys. C, Particles and Fields* **31**, 545 (1986); *Zeit. Phys. C, Particles and Fields* **34**, 255 (1987); SELEX reports.

- [20] D. R. Thompson et al., *Phys. Rev. Lett.* **79** (1997) 1630;
BNL Press Release 97-91 (http://lemond.phy.bnl.gov/e852/home_e852.html)
- [21] D. Alde et al. Proc. of HADRON-97, BNL, August 1997. More references there.
- [22] Yu.D.Prokoshkin and S.A.Sadovsky, *Phys. At. Nucl.* **58** (1995) 606.
- [23] G. M. Beliadze et al., *Phys. Lett.* **B313** (1993) 276-282; A.Zaitsev, Proc. of HADRON-97, BNL, August 1997.
- [24] H. Aoyagi et al., *Phys. Lett.* **B314** (1993) 246-254.
- [25] D. Alde et al., *Phys. Lett.* **B205** (1988) 397.
- [26] B. R. Holstein, *Phys.Rev.D* **53** (1996) 53, 4099.
- [27] M. A. Moinester, Chiral Anomaly Tests, in "Physics with GeV-Particle Beams", Eds. H. Machner, K. Sistemich, World Scientific, 1995, hep-ph/9409307.
- [28] Y.M. Antipov et al., *Phys.Rev.D* **36** (1987) 21.
- [29] R. Edelstein, J. Russ, P. Cooper et al., Fermilab proposal SELEX/E781, <http://fn781a.fnal.gov/>; J. Russ, *Nucl. Phys. A* **585**, 39 (1995).
- [30] T. Jensen et al., *Phys. Rev.* **27D**, 26 (1983).
- [31] J. Huston et al., *Phys. Rev.* **33** (1986) 3199.
- [32] L. Capraro et al., *Nucl. Phys.* **B288** (1987), 659.
- [33] D. Berg et al., *Phys. Lett.* **B98** (1981) 119.
- [34] C. Chandlee et al., *Phys. Rev. Lett.* **51**, 168 (1983).
- [35] S. Cihangir et al., *Phys. Lett.* **117B** (1982) 119, Ibid, p.123; *Phys. Rev. Lett.* **51** (1983) 1.
- [36] V. Steiner, M. A. Moinester, M. Buenerd, POLARIS, A Monte Carlo event generator for polarizability experiments. V. Steiner, M. A. Moinester, ANOMALY, a Monte Carlo event generator for chiral anomaly experiments.
- [37] N.I. Starkov et al., *Sov. J. Nucl. Phys.* **36** (1982) 1212.
- [38] M. Zielinski et al., *Phys. Rev.* **29D** (1984) 2633.
- [39] V. Steiner, M. A. Moinester, et al., FNAL E781 H-741, 1995.
- [40] J. Wess and B. Zumino, *Phys.Lett.B* **37** (1971) 95;
E. Witten, *Nucl.Phys.B* **223** (1983) 422.
- [41] J.Bijnens, *Int. Journal Mod. Phys.A*, **8** (1993) 3045;
J. Bijnens et al. *Phys.Lett.B* **237** (1990) 488; *Z.Phys.C* **46** (1990) 599.